International Journal of Nanoelectronics and Materials
IJNeaM
ISSN 1985-5761 | E-ISSN 2232-1535

Employing Atmospheric Pressure Plasma Jet Technology in Surface Treatment Iron Oxide Films for Industrial Applications

Nisreen kh. Abdalameer [a*], Eman kadum. Jebur [a], Mirvat D. Majed [a], and Rafal H. Jassim [a]

[a]*Department of Physics, College of Science for Women, University of Baghdad, Iraq*
∗ Corresponding author. Tel.: +0-000-000-0000; fax: 0000-0001-5303-398X; e-mail: nisreenka_phys@csw.uobaghdad.edu.iq

Received 31 March 2023, Revised 11 July 2023, Accepted 5 October 2023

ABSTRACT

In this study, pure iron oxide nanostructures were prepared by a physical method (laser-induced plasma) inside a vacuum using a second harmonic laser Nd: YAG with a wavelength of 532 nm, a laser energy of 500 mJ and a number of pulses of 300 pulses per second. The effect of the plasma generated from argon gas under normal atmospheric pressure was studied using a "cold plasma jet" system with an output voltage of 13 kV and a frequency of 50 Hz. Iron oxide nanostructures were exposed to cold plasma for different periods. The optical and structural properties of the nanostructures were measured before and after exposure, and there was a clear change in them, thus improving the properties of the nanostructures for use in industrial applications such as gas sensors, photovoltaic cells, diodes, detectors, and solar cells.

Keywords: *Plasma jet, laser-induced plasma, Iron Oxide, Nd: YAG, Cold plasma*

1. INTRODU0CTION

Nanomaterials represent the most recent and significant advance in scientific understanding and practical applications. In today's world of advanced conducting materials, one of the most vital roles that iron oxide plays is in the improvement of characteristics for prospective applications. Because of their various uses, numerous different strategies for producing FeO nanoparticles have been suggested [1].In recent years, the prominent deposition methods effectively useful for synthesizing ferroxidase (FeO) have included chemical coprecipitation, flow injection, sonochemical, electrochemical, and hydrothermal methods. Other methods include the sol-gel method and sonochemical deposition methods.

On the other hand, the relevance of the morphology of FeO nanostructures in terms of optical properties and the surface features of nanostructure interfaces that govern nano-trapping levels [2]. As a result, the development and production of FeO nanoparticles with various structures are very important. Up to this point, a significant amount of research has been conducted on nanostructured materials made of FeO, each of which has a unique morphology and structure [3]. These materials have been synthesized in various forms, including nanoparticles, nanorods, and nanosheets, and their properties and potential applications have been studied intensively [4]. Except for the hydrothermal technique, which is more effective, less expensive, and rewarding, the majority of the aforementioned synthetic methods are relatively pricey. They typically require high temperatures, high sensitivity, and the application of complex procedures. However, the hydrothermal method is one of the few that does not fall into these categories [5].
The study aims to treat the surfaces of iron oxide films using cold plasma technology by examining their structural, morphological, and optical properties.

1.1 PLASMA

The "fourth state of matter," plasma, is typically observed in the form of an arc or a discharge of bright fluorescent light. Plasma is considered the "fourth state of matter" by the scientific community. In plasma, reactive species include electrons, photons, free radicals, positively or negatively charged ions, and gas molecules or atoms in excited or fundamental states with a net neutral charge are all examples of reactive species found in plasma. Because of this, plasma is often referred to be as “quasi-neutral"[6]. Energizing neutral gas results in the creation of plasma at different temperatures and pressures throughout the processing stage. This plasma may be classified as either thermal (equilibrium) or non-thermal (non-equilibrium), depending on the processing conditions [7]. Upholding the thermodynamic equilibrium of all produced species between 2× 103 K and 3× 104 K requires both a high pressure (more than 105 Pa) and a high-power supply (higher than 50 MV). Non-thermal plasma, on the other hand, does not need a lot of power or pressure to exist, and it may do so even in the absence of a localized thermodynamic equilibrium. For these reasons, it is sometimes referred to as non-equilibrium plasma. There are two distinct types of plasma exist: (i) quasi-equilibrium

plasma, with temperatures between 100 and 150 degrees Celsius and generated species in a state of local thermodynamic equilibrium; and (ii) nonequilibrium plasma, with temperatures between 60 and 100 degrees Celsius and no local thermodynamic equilibrium. In the former, the temperature of electrons is greater than that of heavier species, which is mild (a lower temperature for the entire system) [8].
When an electric field is applied to a neuronal gas at atmospheric pressure, cold plasma, also known as atmospheric pressure plasma, is produced. Between two electrode plates, a gas or gas mixture is exposed to either a direct current (D.C.) or an alternating current (A.C.) at a frequency (varying from Hz to GHz). Three key events are involved in the plasma formation from the neutral gas: excitation, ionization, and dissociation. Few electrons or ions exist in a neutral gas or combination of gases. Electrons and other atoms may collide with free carrier charges when an electric field is applied to the environment. The atoms' translational and transitional energies increase throughout the excitation process. Ionization of atoms follows naturally from releasing electrons that are only weakly linked to nuclei during excitation. When electrons, ions, atoms, and neutral molecules in a gas meet with radiation, ionization and excitation can occur concurrently. Dissociation, on the other hand, is brought about by a molecule's inelastic collision with an electron, ion, or photon.

Corona and dielectric barrier discharges are examples of D.C. and low-frequency discharges that can be classified as atmospheric pressure plasma or cold plasma based on the excitation frequency. APPJ are examples of radiofrequency discharges classified as atmospheric pressure plasma [9].

1.2 PLASMA JET SYSTEM

A plasma plume of atmospheric pressure plasma jet (APPJ) is released into the nearly open environment outside the device via a duct. Any number of APPJs are possible to produce, with variations in electrode layout and power input [10]:

- A plasma jet powered by radiofrequency (RF) may be either capacitively or inductively driven. The two concentric electrodes produce a highly uniform and steady discharge at R.F. power and frequency ranging from 1 to 100 MHz, as shown in Figure 1(a).
- Two ring electrodes are positioned coaxially around the dielectric tube in a DBD-based plasma jet, with the gas flow perpendicular to the electric field generated by the rings (see Figure 1). (b).

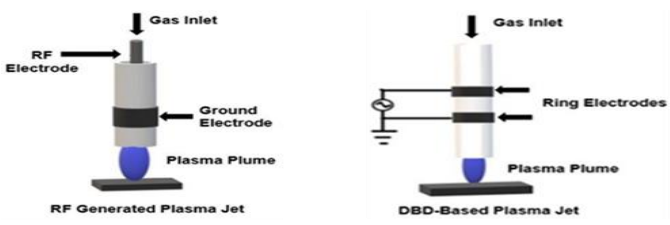

Figure 1 (a) R.F. Generated Plasma Jet, (b)DBD–Based Plasma Jet [11]

1.3 APPLICATION

APPJ has many different applications, including the deposition of coatings, the modification of surfaces, the synthesis of nanoparticles, antimicrobial therapy, relieving itching and pain, repairing damaged skin's protective layer, speeding up the healing process, and minimizing scarring. These are just a few examples of the biological uses of this technique [12].

2.0 PROCEDURE SETUP

2.1 Preparation of thin films

The apparatus used in the experiment was a stainless steel PLD chamber that had been evacuated to a pressure of (2.5× 103) mbar using a molecular turbo pump. The FeO targets were made by first pelletizing FeO powder (Alfa Aesar 99.999 percent) into discs with a diameter of 10 mm and a thickness of around 2 mm using a hydrostatic press set at 8 tons/cm2 and then heating them in the air for 1 h. The target was mounted on a rotatable sample holder to prevent the creation of craters because of laser irradiation. The Nd:YAG laser with a wavelength of 532 nm was the second harmonic, and the repetition rate was set at 6 Hz. The laser energy was set at 500 mJ, and the number of laser pulses was set at 300 shots per second.

2.2 Thin film surface treatment

The usual atmospheric pressure plasma jet system uses argon gas with an A.C. voltage of 175 volts. In addition, the flow rate of argon gas in the system is 3 l/min, where samples were exposed to cold plasma at a distance of 2 cm from the target and for different times (0, 4, 8, 12) min. Figure (2) shows a schematic diagram of the plasma jet system that was used to treat thin film surfaces:

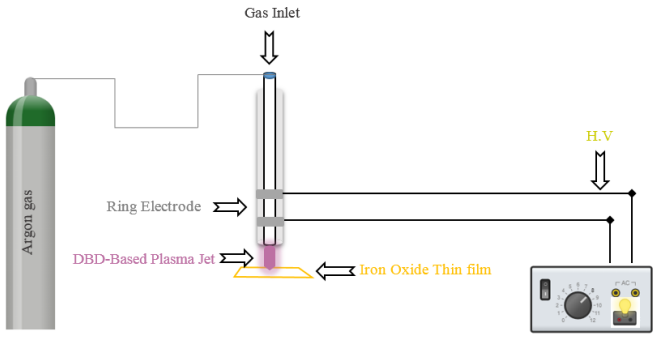

Figure 2 Experimental setup schematic

3. RESULT AND DISCUSSION

3.1 Structure Properties

3.1.1 X-Ray Diffraction analysis:

Using CuK radiation with a wavelength of 1.5406, X-ray diffraction was used to investigate and study the crystalline structure of FeO thin films before and after plasma exposure. The angle 2θ was selected with a step of 0.05 from 5 to 90 degrees. The X-ray diffraction pattern of FeO thin

films is shown in Figure 2 before and after plasma exposure. According to the findings of the XRD, the locations of each peak in the FeO crystal are unique phases according to the JCPDS 86 -0550 label. The absence of any diffraction peaks associated with other phases confirmed its purity. The high purity of the composite films is shown by the absence of peaks relating to other phases or contaminants. The summits are situated at acute angles to one another of 34.25°, 40.21°, 68.57°, and 72.98° right, concerning the (110), (112), (018), and (102) plates, respectively, in the case of unexposed plasmas, as shown in Figure 3a. But when it was exposed to the plasma, new peaks appeared, indicating the crystalline improvement of the films, and this means that the plasma improved its structural properties, as the peak appeared at an angle of 45.56 degrees, corresponding to (116) in addition to an increase in the intensity of the peaks as shown in Figure 3(b, c, and d). After the surface treatment with plasma, when compared to the structure of the FeO thin film before exposure, the structure of the FeO film did not change. However, there was a little shift in the position of the peaks, which indicates that the network parameters shrank. This may have something to do with the structural relaxing and flaw removal that occur after plasma application [13].

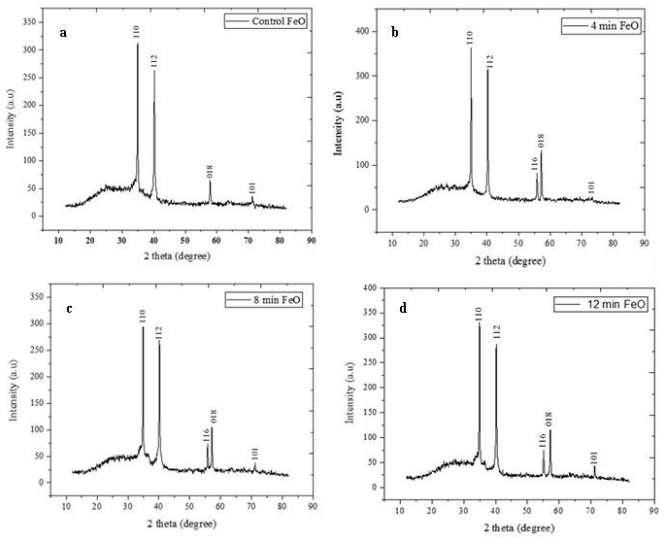

Figure 3 XRD pattern of thin films (a) before plasma treatment, (b) after 4 min of plasma treatment, (c) after 8 min of plasma treatment,and (d) after 12 min of plasma treatment

3.2 Topographic properties

3.2.1 Atomic Force Microscope

The surface morphology of FeO thin films generated before and after plasma treatment was investigated with the help of pictures obtained from atomic force microscopy (AFM). The AFM (2D) picture of the FeO layer in Fig. 4(a) reveals that the shape is consistent across the layer. An AFM image is also used to measure the root mean square (RMS) of the roughness plane, and the result is displayed in Fig. 4b as having a value of 78.25 nm. Following plasma treatment, an AFM picture of the FeO layer in two dimensions is shown in Figure 5a. By evaluating the AFM images (3D) taken before and after the plasma treatment shown in Figures (4, 5, 6, and 7) for the times (0, 4, 8, and 12), respectively. The morphology of the films before plasma treatment is noticeably different from the morphology of the films after plasma treatment. After being treated with the plasma jetting method, the composite thin films now contain much bigger granules (a nanopyramid pattern) and an apparent higher porosity. Before this, the composite thin films formed densely compacted micro-granules and eventually a smooth surface. This increase in grain size is attributable to the radiative stress that results from the bombardment of photons, ions, and atoms caused by the activation of plasma.

On the contrary, a larger porosity might be preferable for anticipated photoelectrochemical uses. It is a well-known fact that the scattering and penetration of light increase as the surface area of a material increases due to porosity. Larger grains also limit the recombination of electron-hole pairs in the opposite direction [14]. This film's roughness (RMS) was measured to be 41.0, 33.15, and 25.47 nm, respectively.

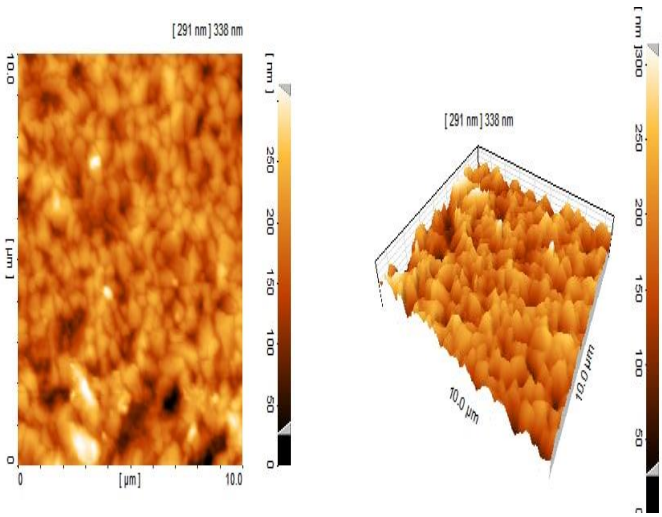

Figure 4 Topography Properties of FeO films (a) before plasma exposure (2D), (b) before plasma exposure (3D)

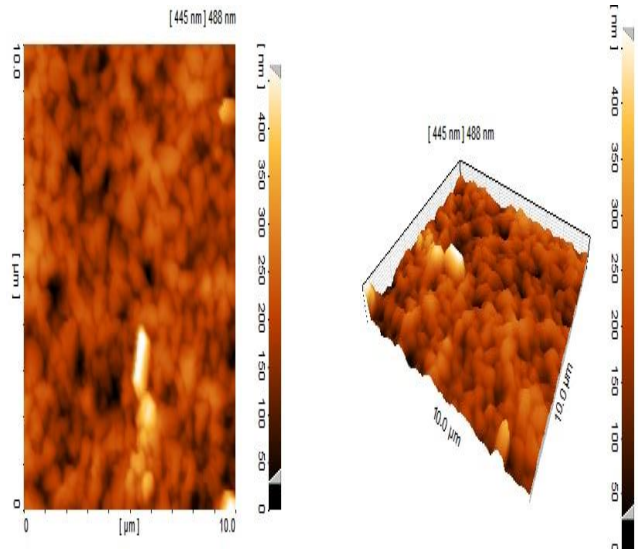

Figure 5 Topography Properties of FeO films (a) after plasma exposure at t = 4 min (2D), (b) after plasma exposure at t = 4 min (3D)

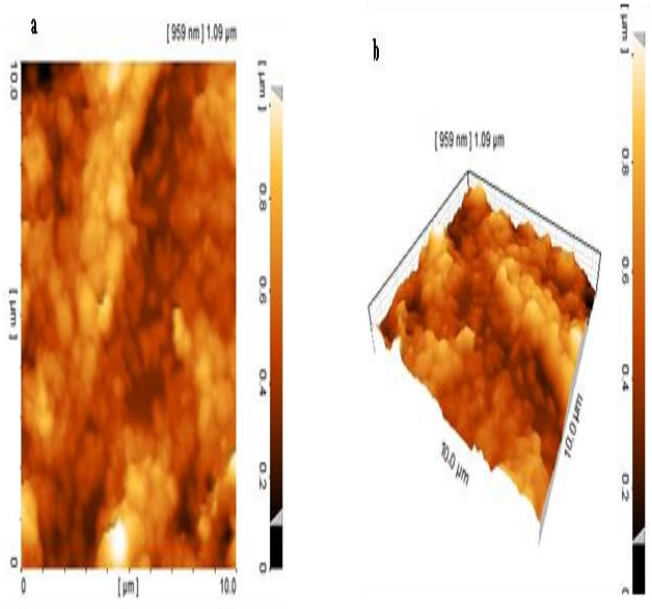

Figure 6 Topography Properties of FeO Films (a) after plasma exposure at t = 8 min (2D), (b) after plasma exposure at t = 8 min (3D)

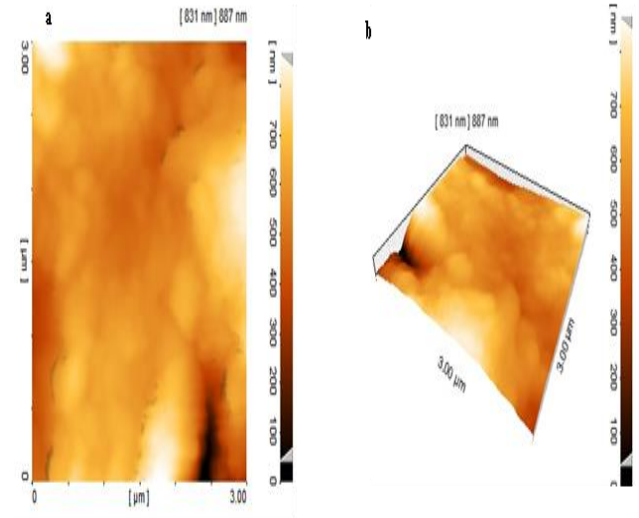

Figure 7 Topography Properties of FeO films (a) after plasma exposure at t = 12 min (2D), (b) after plasma exposure at t = 12 min (3D)

3.3 Optical properties

3.3.1 Absorption

Figure 8 displays the absorption spectra of the unexposed and exposed plasma films at various intervals, which were obtained using a UV-visible recording spectrophotometer (Shimadzu 1700 UV-2601 PC, software 1650) to determine the films' optical characteristics. Very identical behavior can be seen between the spectral lines of the untreated sample and the three plasma-treated samples; the only difference is that absorbance rises with longer exposure times. Figure 8 shows the spectrum of absorption as a function of wavelength.

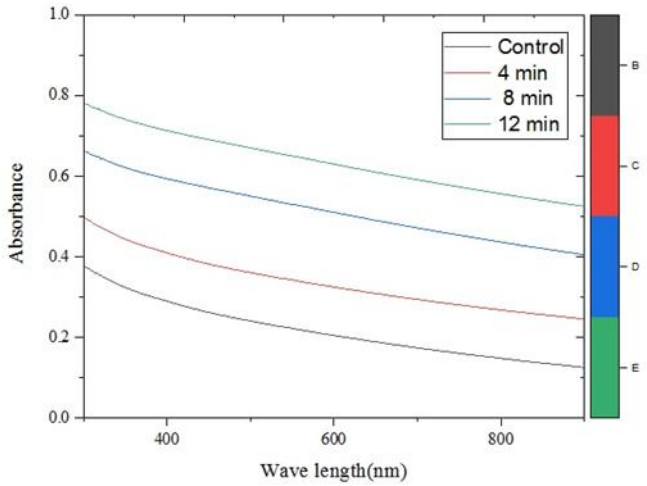

Figure 8 Differences in absorption spectra between untreated FeO films and those treated for varying amounts of time

3.3.2 Transmission

Figure 9 demonstrates the difference in transmittance spectra between those taken before and after plasma treatment. It was found that the transmittance decreased because increasing the concentration of the granules leads to higher light scattering [15].

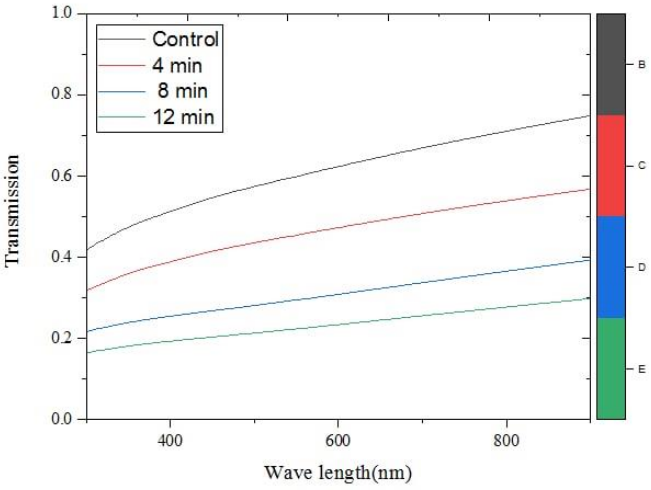

Figure 9 Spectra of transmission through untreated and treated FeO films exposure time

3.3.3 Optical energy gap

The Tauc's relation may be used to compute the coefficient of absorption [16]:

$\alpha h\vartheta = B(h\vartheta - E_g)^n$ ……(1)

By plotting $(\alpha h\vartheta)^2$ against the energy of a photon $h\vartheta$, and extending the straight part of the resulting curve to cut the $h\vartheta$ axis at the point where $(\alpha h\vartheta)^2 = 0$, you can find the Energy gap (Eg).

Iron oxide (FeO) films' optical energy gap before and after exposure to non-thermal plasma for 4, 8, and 12 minutes is seen in Figure 10. Time spent in a non-thermal plasma has been proven to steadily diminish the optical energy gap.

Before being exposed to a non-thermal plasma, the energy gap was 3.48 eV. While the energy gap was 3.19, 2.86, and 2.51 eV after exposure to non-thermal plasma for 4, 8, and 12 minutes, respectively.

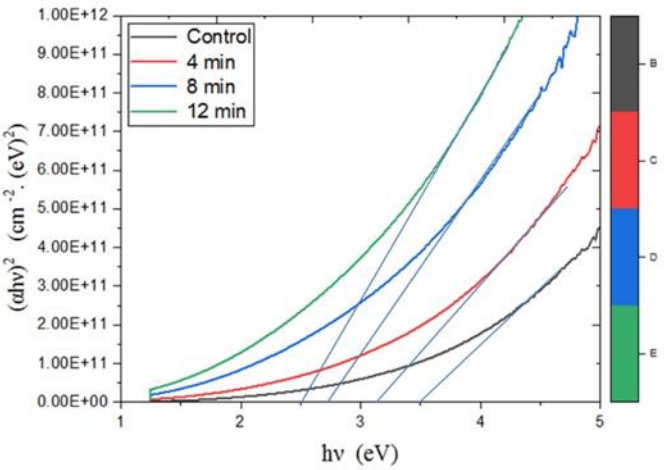

Figure 10 The energy gap is a function of photon energy for untreated FeO films and those treated with different exposure time

5. CONCLUSION

In this study, the surfaces of iron oxide films were treated with cold plasma to improve the structural, topographic, and optical properties of films exposed to plasma for varying amounts of time before and after preparation. It was observed that there was a crystalline improvement in the structure of the films exposed to cold plasma through crystallization peaks, The morphology of the layer surfaces was analyzed using AFM microscopy. Findings from studies. The findings showed that following plasma treatment, the molecules clumped together. The plasma treatment reduced the outer layer roughness, thus yielding a thin hydrophilic FeO film. By studying the optical properties, the study proved that the electron transfer and stimulation process from the valence beam to the conduction beam is limited to the permissible direct electronic transitions only and that the transmittance values decrease. At the same time, the absorbance increases with the exposure time to the plasma.

REFERENCES

[1] S. F. Hasany, N. H. Abdurahman, A. R. Sunarti, and R. Jose, "Magnetic Iron Oxide Nanoparticles: Chemical Synthesis and Applications Review," *CNANO*, vol. 9, no. 5, pp. 561–575, 2013.

[2] K. Sharma, I. Katyal, A. Srivastava, V. Raghavendra Reddy, and A. Gupta, "Synthesis and Characterization of GaO(O.H.)–FeO(O.H.) Nanorod Composite Prepared via Hydrothermal Method," in *Recent Trends in Materials and Devices*, V.K. Jain, S. Rattan, and A. Verma, Eds., Springer Proceedings in Physics, vol. 256, Singapore: Springer, 2020, pp. 10^2.

[3] S. Laurent, D. Forge, M. Port, A. Roch, C. Robic, L. Vander Elst, and R.N. Muller, "Magnetic Iron Oxide Nanoparticles: Synthesis, Stabilization, Vectorization, Physicochemical Characterizations, and Biological Applications," *Chem. Rev.*, vol. 108, no. 6, pp. 2064–2110, 2008.

[4] L. Storozhuk, M.O. Besenhard, S. Mourdikoudis, A.P. LaGrow, M.R. Lees, L.D. Tung, A. Gavriilidis, and N.T.K. Thanh, "Stable Iron Oxide Nanoflowers with Exceptional Magnetic Heating Efficiency: Simple and Fast Polyol Synthesis," *ACS Appl. Mater. Interfaces*, vol. 13, no. 38, pp. 45870–45880, 2021.

[5] M.V. Zyuzin, M. Cassani, M.J. Barthel, H. Gavilan, N. Silvestri, A. Escudero, A. Scarpellini, F. Lucchesi, F.J. Teran, W.J. Parak, and T. Pellegrino, "Confining Iron Oxide Nanocubes inside Submicrometric Cavities as a Key Strategy To Preserve Magnetic Heat Losses in an Intracellular Environment," *ACS Appl. Mater. Interfaces*, vol. 11, no. 45, pp. 41957–41971, 2019.

[6] Yasoob A, N., Abdalameer, N.K., Mohammed, A.Q., "Plasma Production and Applications: A Review," *Int. J. Nanosci.*, vol. 21, no. 6, 2022. .

[7] E.K. Jebur, "Effect of the Dielectric Barrier Discharge Plasma on the Optical Properties of CdS Thin Film," *Baghdad Sci. J.*, vol. 16, no. 4, pp. 1030–1035, 2019. .

[8] N.K. Abdulameer, "Impact of Dielectric Barrier Discharge (DBD) Plasma on the Optical Properties of Thin Films," *J. Eng. Appl. Sci.*, vol. 15, no. 8, pp. 1937–1942, 2020. .

[9] S.K. Pankaj, C. Bueno-Ferrer, N. Misra, P. Bourke, and P. Cullen, "Zein film: Effects of dielectric barrier discharge atmospheric cold plasma," *J. Appl. Polym. Sci.*, vol. 131, 2014. .

[10] C.M.G. Charoux, L. Free, L.M. Hinds, R.K. Vijayaraghavan, S. Daniels, C.P. O'Donnell, and B.K. Tiwari, "Effect of non-thermal plasma technology on microbial inactivation and total phenolic content of a model liquid food system and black pepper grains," *LWT*, vol. 118, 2020.

[11] H. Turkoglu Sasmazel, M. Alazzawi, and N. Kadim Abid Alsahib, "Atmospheric Pressure Plasma Surface Treatment of Polymers and Influence on Cell Cultivation," *Molecules*, vol. 26, no. 6, p. 1665, Mar. 2021.

[12] H. Tolouie, M.A. Mohammadifar, H. Ghomi, and M. Hashemi, "Cold atmospheric plasma manipulation of proteins in food systems," *Crit. Rev. Food Sci. Nutr.*, vol. 58, pp. 2583–2597, 2018.

[13] H.G. Drickamer, R.W. Lynch, R.L. Clendenen, and E.A. Perez-Albueene, "X-Ray Diffraction Studies of the Lattice Parameters of Solids under Very High Pressure," *Solid State Physics - Advances in Research and Applications*, vol. 19, pp. 135–228, 1967.

[14] S.A. Hussain, A.J. Radi, F.A. Najim, and M.A. Shaheed, "Structural, Optical and Sensing Properties of ZnO:Cu Films Prepared by Pulsed Laser Deposition," *J. Phys.: Conf. Ser.*, vol. 1591, p. 012088, 2020.

[15] A. Larena, F. Millán, G. Pérez, and G. Pinto, "Effect of surface roughness on the optical properties of multilayer polymer films," *Appl. Surf. Sci.*, vol. 187, nos. 3-4, pp. 339–346, 2002.

[16] S.N. Mazhir, N.A. Abdullah, H.I. Al-Ahmed, N.H. Harb, and N.K. Abdalameer, "The effect of gas flow on plasma parameters induced by microwave," *Baghdad Sci. J.*, vol. 15, no. 2, pp. 205–210, 2018.